JOC The Journal of Organic Chemistry

Article

pubs.acs.org/joc

Theoretical Prediction of One- and Two-Photon Absorption Properties of *N*-Annulated Quaterrylenes as Near-Infrared Chromophores

Xiao-Ting Liu,[†] Jing-Fu Guo,[‡] Ai-Min Ren,*[,†] Shuang Huang,[†] and Ji-Kang Feng[†]

[†]State Key Laboratory of Theoretical and Computational Chemistry, Institute of Theoretical Chemistry, Jilin University, Changchun, 130023, People's Republic of China

[‡]School of Physics, Northeast Normal University, Changchun, 130021, People's Republic of China

Supporting Information

ABSTRACT: Graphene nanoribbons (GNRs) have attracted increasing attention due to high potentiality in nanoelectronics. In the present study, quantum-chemical calculations of structural and nonlinear optical properties have been first carried out for the nanoelectronical materials, a new series of ladder-type *N*-annulated quaterrylenes and their imide chromophores. The effects of the solvent, terminal groups, the number of *N*-annulated bridges, and π-conjugated length are discussed in detail. The solvent effect is significant on the one-photon absorption (OPA). Moreover, the OPA and two-photon absorption (TPA) properties of the two series of DI and N-MI molecules show a clear solvent dependence, which is attributed to the carboximide substitution featuring larger polarization. Introducing electron-donating groups and dicarboximides and increasing the conjugated length lead to red-shifts of the OPA, emission, and TPA spectra, lower emission lifetimes, and enhanced TPA cross sections (δ_{max}), but further extension of the conjugated framework does not always promote an increase of δ_{max}. The changing trends of δ_{max} can be explained by the transition moment and the intramolecular charge transfer. All *N*-annulated quaterrylene and their imide derivatives possess small energy gaps, intense near-infrared absorption and emission, and large δ_{max}, which are important for use as two-photon fluorescent labeling materials.

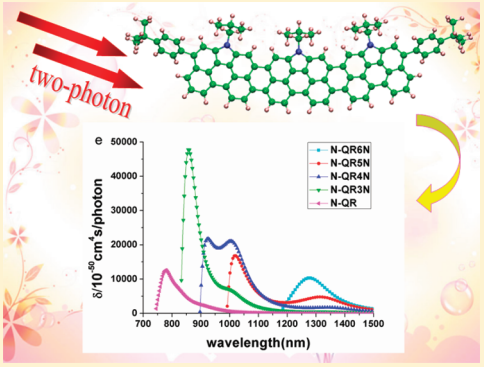

INTRODUCTION

The development of new organic compounds with efficient two-photon absorption (TPA) properties and highly fluorescent quantum yields (Φ) is a subject of broad scientific and technological interest for a variety of applications including optical limiting,[1] three-dimensional (3D) fluorescence microscopy,[2] photodynamic therapy,[3] two-photon fluorescent labeling,[4] and frequency up-converted lasing.[5] For all of these applications, TPA dyes possessing large two-photon absorption cross sections (δ_{max}) in the near-infrared (NIR) region are highly desirable.

Graphene nanoribbons (GNRs) have attracted increasing attention due to high potentiality in nanoelectronics based on GNR. Rylene and its dicarboxylic imide chromophores and poly(peri-naphthalene) with an extended aromatic π-system are used to construct GNRs, which can be regarded as structurally perfect GNRs. This could be attributed to their exceptional chemical, thermal, and photochemical stabilities, nontoxicity, and high extinction coefficients.[6] Thanks to their excellent properties, they have been explored for applications as optoelectronic,[7] photovoltaic[8] and molecular devices,[9] energy transfer cascades,[10] sensitizers in solar cells,[11] and NIR absorbing dyes.[12] Recently, their applicability in optical power limiting and up-conversion lasing has been successfully demonstrated.[13] In addition, some perylene dyes were studied theoretically by our group.[14] The experimental and computational results show that rylenes and their derivatives exhibit large TPA cross sections in the NIR region and also are ideally suited as high-performance fluorescent labels for biologically active probes. It is known that TPA fluorescent probes should have some special properties, such as high sensitivity and selectivity, good solubility, large TPA cross sections, and high fluorescence quantum yield. Only a few water-soluble rylene and diimide derivatives have so far been reported. To date, for improving their solubility, there have been some strategies including incorporation of the phenoxy groups at the bay positions of the terminal naphthalene units,[15] substitution with either electron-donating or electron-withdrawing character,[16] and introduction of *S*-heterocylic annulated perylene.[17] Additionally, *N*-annulated perylene, in which the nitrogen atoms are annulated at the bay position, becomes one option for such a purpose because additional flexible alkyl chains can be easily introduced by alkylation reaction and can thus improve the solubility.[18] Also the electron-donating character of amines can increase the electron density of the entire π-system and lead to novel opto-electronic properties. Some *N*-annulated perylenes have been reported by Wang group[18] and Wu group.[19] Very

Received: October 20, 2011
Published: November 28, 2011

recently, several bis *N*-annulated quaterrylenes possessing good solubility, high Φ, strong absorption and emission intensity in the NIR region have been also synthesized.[18c,19a]

To the best of our knowledge, up to now, the nonlinear optical properties of *N*-annulated quaterrylene derivatives have remained unclear. Herein, we focused on the influence of the solvent, electron-donating and -accepting strength, π-conjugated length, and the number of nitrogen bridges on their TPA properties. The aim of the present theoretical studies is to construct well-defined functionalized TPA materials. The intrinsic correlations between the molecular structures and TPA properties were revealed, and several new *N*-annulated quaterrylene derivatives with high δ_{max} were designed. We hope our theoretical investigation will provide a new insight into the design of new *N*-annulated rylene dyes that can eventually be explored as two-photon absorption fluorescent labeling chromophores.

COMPUTATIONAL DETAILS

In this study, all of the calculations were carried out with the Gaussian 09 program package.[20] The ground-state geometries of all molecules were fully optimized without any symmetric constraints by using the density functional theory (DFT) with the 6-31G(d) basis set and the B3LYP hybrid functional.[21] Vibrational analyses were carried out to ensure that the minimums of the ground state were reached on the potential energy surfaces. On the basis of each optimized structure, the electronic absorption spectra were systematically investigated by time-dependent density functional theory (TDDFT) at the same level. Moreover, the effect of solvent was taken into account by using the polarized continuum model (PCM) approach.[22] For the sake of the comparison, other functionals in TD-DFT were employed for calculating compounds **DI** and **N-QR** and the results were summaried in Table 1. As clearly shown in Table 1, the calculated absorption

Table 1. One-Photon Absorption Spectra for DI and N-QR with the Different TD-DFT Methods

	DI		N-QR	
method	λ^{O}_{max}/nm	*f*	λ^{O}_{max}/nm	*f*
TPSSH/6-31G*	732.3	1.66	685.3	1.45
B3LYP/6-31G*	710.0	1.72	664.5	1.51
B3PW91/6-31G*	706.6	1.73	661.5	1.51
CAM-B3LYP/6-31G*	615.0	2.00	575.4	1.75
B3LYP/6-31G* (in chloroform)	752.0	1.97	698.6	1.71
experiment data	760		685	

spectra of chromophores **DI** and **N-QR** obtained by B3LYP/6-31G* in solvent are 752.0 and 698.6 nm, which are in good agreement with the experimental data (760 and 685 nm), respectively.[19a] This makes us confident that the choice of B3LYP for the system is appropriate. The lowest singlet excited-state geometry and the emission spectra were also predicted by employing the TDDFT//B3LYP/6-31G(d) method.

The OPA properties of the studied molecules were also performed by employing the Zerner's intermediate neglect of differential overlap (ZINDO) program including single and double electronic excitation configuration interactions.

The TPA process corresponds to simultaneous absorption of two photons. The TPA efficiency of an organic molecule, at optical frequency $\omega/2\pi$, can be characterized by the TPA cross section $\delta(\omega)$. It can be directly related to the imaginary part of the third-order polarizability $\gamma(-\omega;\omega,-\omega,\omega)$ by[23,24]

$$\delta(\omega) = \frac{3\hbar\omega^2}{2n^2c^2\varepsilon_0} L^4 \mathrm{Im}[\gamma(-\omega;\omega,-\omega,\omega)] \quad (1)$$

in which $\gamma(-\omega;\omega,-\omega,\omega)$ is the third-order polarizability, $\hbar\omega$ is the energy of incoming photons, *c* is the speed of light, ε_0 is the vacuum electric permittivity, *n* denotes the refractive index of medium, and *L* corresponds to the local-field factor. In the calculations presented here, *n* and *L* are set to 1 because of an isolated molecule in vacuum.

The sum-over-states (SOS) expression to evaluate the components of the second hyperpolarizability $\gamma_{\alpha\beta\gamma\delta}$ (α, β, γ, and δ refer to the molecular axis) can be deduced using perturbation theory. By considering a Taylor expansion of energy with respect to the applied field, the Cartesian components $\gamma_{\alpha\beta\gamma\delta}$ are given by refs 25 and 26.

To compare the calculated δ value with the experimental data measured in solution, the damping factor (Γ_K) of excited state *K* in the SOS expression is set to 0.14 eV,[14a,27,28] and the orientationally averaged (isotropic) value of γ is evaluated, which is defined as

$$\langle\gamma\rangle = \frac{1}{15}\sum_{i,j}(\gamma_{iijj} + \gamma_{ijij} + \gamma_{ijji}) \quad i,j = x,y,z \quad (2)$$

Taking the imaginary part of <γ> value into the expression (1), $\delta(\omega)$ can be obtained in comparison with the experimental value.

In principle, any kind of self-consistent field molecular orbital procedure combined with the configuration interaction (CI) can be implemented to calculate the physical parameters in the above expression. In the present work, the properties of electronic excited states were obtained by single and double electronic excitation configuration interactions (SDCI) by means of the ZINDO program. Moreover, the transition energies and transition moments were also obtained in the calculation. Then, the FTRNLO program compiled by our group was used to calculate the second hyperpolarizability and two-photon absorption cross section.

RESULTS AND DISCUSSION

1. Molecular Design and Geometry Optimization. As reported, several methods have been successfully used for enlarging the TPA cross section, such as increasing the donor and acceptor strength, extending the conjugation length, increasing the molecular planarity, changing the conjugation bridge character, enhancing the effective electronic coupling, and increasing the intramolecular charge transfer (ICT).[28−33] To improve the linear and nonlinear optical properties, a series of ladder-type *N*-annulated quaterrylenebis(dicarboximide) chromophores were built by taking into account the above design strategies. The molecular structures are presented in Figure 1. Chromophores **N-QR**, **N-QRN**, **N-QRT**, and **N-QRNPh** are modified by incorporating 4-*tert*-butylphenyl, naphthalene, 2,6-diisopropylphenyl, and di-*p*-tolylamino electron donors in the terminal groups based on molecule **Center**. By introducing dicarboxylic imides into molecule **Center**, molecule **Center11** is constructed. Tri-*N*-annulated hexarylene **N-QR3N** is an elongated π-system by adding one *N*-annulated perylene unit as compared to **N-QR**. **DI** and **DI-NS** feature the electron-donating and -withdrawing terminal groups with respect to molecule **Center11**. Molecules **DI-3N-trans** and **DI-3N-cis** are designed in order to study the effect of adding one nitrogen bridge at the central bay position on the optical properties and take *trans*- and *cis*-isomers into account. The series of N-MI molecules have an *N*-annulated perylene unit at one end and a perylene diimide moiety at the other end. Molecule **N-MI2N** keeps the similar center to **N-MI** except for bearing one nitrogen bridge at the *peri*-position of rylene on the long axis. The other N-MI molecules (**N-MICF**, **N-MIF**, and **N-MIN**) have no nitrogen bridge in the central bay position which is adjacent to the perylene diimide moiety. These structural modifications may bring an improvement effect on the photophysical properties. All of the studied molecules belong to typical donor−donor (D-D), donor−acceptor (D-A), or acceptor−donor−donor−acceptor (A-D-D-A) motifs.

dx.doi.org/10.1021/jo202154h | J. Org. Chem. 2012, 77, 585−597

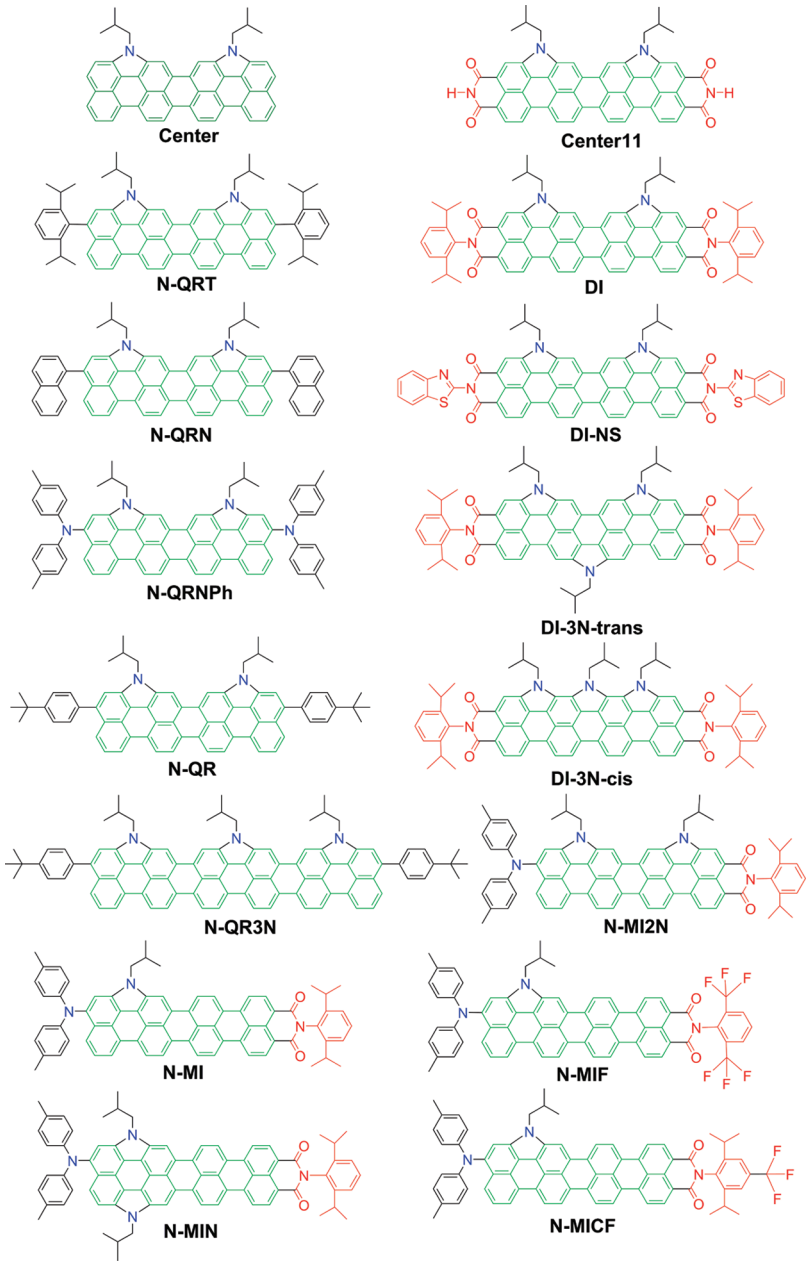

Figure 1. Molecular structures of all compounds studied.

The optimized ground-state geometries of all molecules are stable and verified by the frequency calculations, where no imaginary frequency is found. Additionally, the inclusion solvent was considered. Taking molecules **N-QR**, **DI**, and **N-MI** as examples, they were optimized in chloroform by performing DFT/PCM//B3LYP/6-31G*. The results imply that there are hardly any differences for the geometrical structures between *in vacuo* and in chloroform. So the solvent influence on the molecular geometry can be ignored in the computational process. The optimization results show that the center moieties remain nearly planar except for chromophores **DI-3N-trans** and **N-MIN** whose central cores are deviated from the main body plane (see Figure 2). Due to the steric hindrance, the aryl terminal groups of the molecules are nearly perpendicular to the main body. The geometry changes are expected to have a substantial influence on the electro-optical properties.

2. Electrochemical Properties. The frontier orbital energy levels (four occupied orbitals, four unoccupied orbitals, and energy gap ($\Delta E_{H\text{-}L}$) between the highest occupied molecular orbital (HOMO) and the lowest unoccupied molecular orbital (LUMO)) were estimated from the optimized results. The energy levels are shown in Table 2. As can be seen, the introduction of donor or acceptor groups in the molecule **Center** is an effective way to lower the energy gap and consequently tunes the absorption spectra to longer wavelengths (discussion in the next section). Incorporating electron donors in molecule **Center** leads to decrease in the $\Delta E_{H\text{-}L}$ values in the order **Center** > **N-QRN** > **N-QRT** > **N-QR** > **N-QRNPh** (Table 2), but their differences are very small. That is to say, the HOMO and LUMO energies of the series of NQR compounds depend on the *N*-annulated quaterrylene central core. Evidently, the *N*-annulated quaterrylenes feature a high-lying HOMO energy levels and the *N*-annulated quaterrylene diimides has a

dx.doi.org/10.1021/jo202154h | *J. Org. Chem.* 2012, 77, 585–597

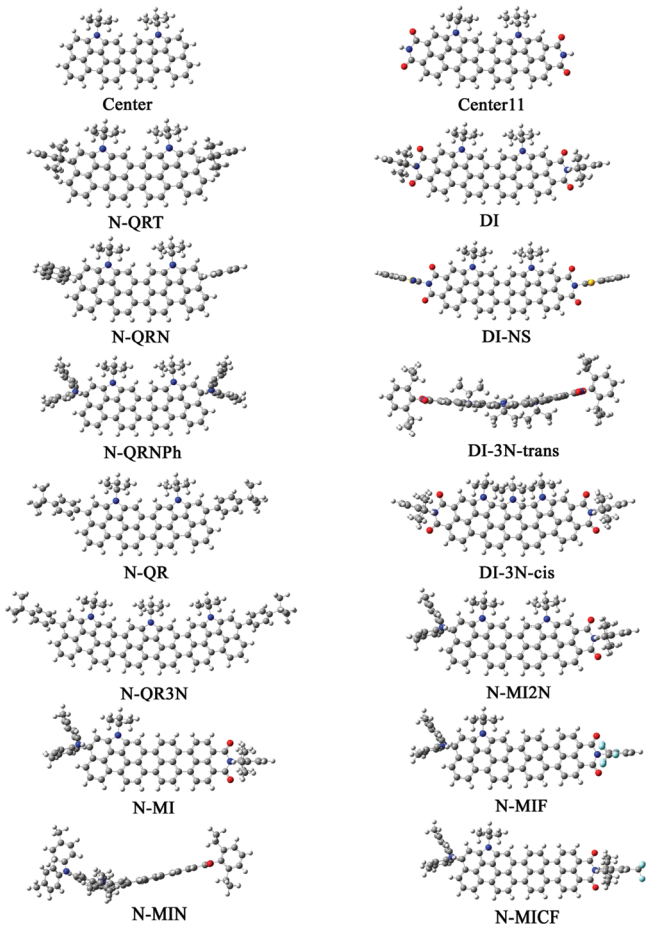

Figure 2. Optimized ground-state geometries of all molecules in this work.

low-lying LUMO energy levels. As a result, the $\Delta E_{H\text{-}L}$ of *N*-annulated quaterrylenes are larger than that of their corresponding diimides, such as **Center** (2.02 eV) > **Center11** (1.80 eV), and **N-QRT** (1.99 eV) > **DI** (1.79 eV), indicating that the *N*-annulated quaterrylene diimides exhibit smaller band gaps. And the energy gaps of *N*-annulated quaterrylene diimides are quite similar regardless of their terminal groups with electron-acceptors or -donors. By replacing the di-p-tolylamino substituent of **N-QRNPh** with the imide and 2,6-diisopropylphenyl moieties at the terminal, the HOMO and LUMO energy levels are both decreased in the order of **N-QRNPh**, and **N-MI2N**. And the energy gaps decrease following the order **N-QRNPh** (1.89 eV) > **N-MI2N** (1.78 eV). This implies that molecule **N-QRNPh** can be the most easily oxidized by many oxidants and molecule **N-MI2N** exhibits lower LUMO energy than **N-QRNPh** which demonstrates that it is electron-rich by electron delocalization along the large π-conjugated framework. The $\Delta E_{H\text{-}L}$ decreases with the number of the *N*-annulation bridge reduced on the short or long axis, such as **DI-3N-cis** (2.01 eV) > **DI** (1.79 eV), **N-MIN** (1.76 eV) > **N-MI** (1.67 eV) and **N-MI2N** (1.78 eV) > **N-MI** (1.67 eV). Comparing molecules **N-MI** with its analogues **N-MICF** and **N-MIF**, the terminal groups of which are modified by the strong electron-acceptor "fluorine atoms", we can find that the $\Delta E_{H\text{-}L}$ does hardly change. But the HOMO and LUMO energy levels of molecule **N-MICF** are simultaneously tuned to the lowest among the N-MI series, indicative of the strong electron affinity of the *p*-CF_3 group. The energy of HOMO increases with the π-conjugation length extended, that is, **N-QR** (−4.12 eV) < **N-QR3N** (−3.91 eV), and the energy of LUMO decreases, that is, **N-QR** (−2.16 eV) > **N-QR3N** (−2.41 eV). Consequently, the energy gap deceases with the extension of conjugation length (1.96 eV (**N-QR**) > 1.50 eV (**N-QR3N**)). This identifies the fact that extending the π-conjugation length makes molecule **N-QR3N** easily oxidized. Specially, **DI-3N-cis** exhibits larger energy gap than **DI-3N-trans**, which may be ascribed to the distort structure of **DI-3N-trans**.

3. One-Photon Absorption and Emission Properties.

Calculations of the one-photon absorption and emission properties were performed by means of the TD-DFT//B3LYP/6-31G* approach on the basis of the optimized geometry. In addition, the effect of solvent was taken into account at the same level. The maximum OPA wavelengths (λ^{O}_{max}), the emission wavelengths (λ^{E}_{max}), transition energies (E_{Flu}), oscillator strengths (f), transition nature, emission lifetimes (τ), and some experimental data for each molecule are all collected in Table 3. For comparison, the calculated absorption spectra of chromophores **N-QR**, **DI**, and **N-QRN** in gas are shorter by 20−50 nm than the experimental values. Additionally, as the solvent effect

Table 2. Calculated Frontier Orbital Energy by the B3LYP/6-31G* Method[a]

molecule	H−3	H−2	H−1	H	L	L+1	L+2	L+3	ΔE_{H-L}
Center	−5.63	−5.56	−5.34	−4.18	−2.16	−1.02	−0.59	−0.27	2.02
Center11	−6.33	−6.26	−6.09	−5.02	−3.22	−2.28	−1.54	−1.46	1.80
N-QRNPh	−5.53	−4.98	−4.76	−4.08	−2.19	−1.08	−0.64	−0.31	1.89
N-QR	−5.62	−5.55	−5.21	−4.12	−2.16	−1.06	−0.68	−0.30	1.96
N-QRT	−5.68	−5.60	−5.35	−4.20	−2.21	−1.09	−0.64	−0.33	1.99
N-QRN	−5.64	−5.58	−5.33	−4.19	−2.19	−1.08	−0.97	−0.97	2.00
N-QR3N	−5.56	−5.44	−4.69	−3.91	−2.41	−1.64	−0.91	−0.81	1.50
DI	−6.16	−6.15	−6.05	−4.99	−3.20	−2.26	−1.53	−1.44	1.79
DI-NS	−6.25	−6.24	−6.14	−5.09	−3.30	−2.35	−1.64	−1.53	1.79
DI-3N-trans	−6.11	−5.98	−5.70	−4.92	−3.07	−2.18	−1.42	−1.25	1.85
DI-3N-cis	−6.13	−6.06	−5.89	−4.93	−2.92	−2.18	−1.45	−1.13	2.01
N-MI2N	−5.90	−5.79	−5.15	−4.50	−2.72	−1.70	−1.11	0.84	1.78
N-MI	−6.00	−5.85	−5.21	−4.57	−2.90	−1.80	−1.21	−0.93	1.67
N-MIF	−5.99	−5.85	−5.20	−4.57	−2.90	−1.80	−1.22	−0.92	1.67
N-MICF	−6.06	−5.93	−5.27	−4.64	−2.98	−1.88	−1.30	−1.01	1.66
N-MIN	−5.75	−5.52	−5.12	−4.53	−2.77	−1.55	−1.20	−0.83	1.76

[a]H denotes the HOMO and L denotes the LUMO; units in eV.

dx.doi.org/10.1021/jo202154h | J. Org. Chem. 2012, 77, 585−597

Table 3. One-Photon Absorption and Excitation Properties (TDDFT)

molecule	λ^{O}_{max}/nm	f	transition nature	λ^{E}_{max}/nm	E_{Flu}/eV	f	transition nature	τ/ns
Center	635.7	1.07	$S_0 \rightarrow S_1$ (H)→(L) 37%	702.2	1.77	1.04	$S_1 \rightarrow S_0$ (H)→(L) 51%	7.09
	670.3[a]	1.31	$S_0 \rightarrow S_1$ (H)→(L) 39%					
Center11	698.9	1.45	$S_0 \rightarrow S_1$ (H)→(L) 51%	760.8	1.63	1.41	$S_1 \rightarrow S_0$ (H)→(L) 51%	6.16
	750.5[a]	1.76	$S_0 \rightarrow S_1$ (H)→(L) 50%					
N-QRNPh	704.8	1.44	$S_0 \rightarrow S_1$ (H)→(L) 49%	785.2	1.58	1.44	$S_1 \rightarrow S_0$ (H)→(L) 50%	6.42
	742.9[a]	1.67	$S_0 \rightarrow S_1$ (H)→(L) 50%					
N-QR	664.5	1.51	$S_0 \rightarrow S_1$ (H)→(L) 37%	738.2	1.68	1.50	$S_1 \rightarrow S_0$ (H)→(L) 51%	5.45
	698.6[a]	1.71	$S_0 \rightarrow S_1$ (H)→(L) 39%	700[b]				
	685[b]							
N-QRT	654.1	1.36	$S_0 \rightarrow S_1$ (H)→(L) 50%	725.3	1.71	1.32	$S_1 \rightarrow S_0$ (H)→(L) 51%	5.98
	687.4[a]	1.57	$S_0 \rightarrow S_1$ (H)→(L) 50%					
N-QRN	650.7	1.40	$S_0 \rightarrow S_1$ (H)→(L) 37%	724.6	1.71	1.40	$S_1 \rightarrow S_0$ (H)→(L) 51%	5.64
	680.2[c]	1.59	$S_0 \rightarrow S_1$ (H)→(L) 39%	694[b]				
	673[b]							
N-QR3N	848.5	2.52	$S_0 \rightarrow S_1$ (H)→(L) 35%	928.9	1.33	2.52	$S_1 \rightarrow S_0$ (H)→(L) 51%	5.20
	911.9[a]	2.77	$S_0 \rightarrow S_1$ (H)→(L) 38%					
DI	710.0	1.72	$S_0 \rightarrow S_1$ (H)→(L) 36%	774.8	1.60	1.68	$S_1 \rightarrow S_0$ (H)→(L) 51%	5.37
	752.0[a]	1.97	$S_0 \rightarrow S_1$ (H)→(L) 38%	775[b]				
	760[b]							
DI-NS	708.9	1.76	$S_0 \rightarrow S_1$ (H)→(L) 36%	772.7	1.60	1.71	$S_1 \rightarrow S_0$ (H)→(L) 51%	5.27
	756.3[a]	2.03	$S_0 \rightarrow S_1$ (H)→(L) 39%					
DI-3N-trans	690.2	1.69	$S_0 \rightarrow S_1$ (H)→(L) 37%	744.1	1.67	1.67	$S_1 \rightarrow S_0$ (H)→(L) 51%	4.96
	728.6[a]	1.96	$S_0 \rightarrow S_1$ (H)→(L) 39%					
DI-3N-cis	656.9	1.57	$S_0 \rightarrow S_1$ (H)→(L) 39%	708.7	1.75	1.54	$S_1 \rightarrow S_0$ (H)→(L) 50%	4.90
	689.9[a]	1.84	$S_0 \rightarrow S_1$ (H)→(L) 41%					
N-MI2N	738.1	1.47	$S_0 \rightarrow S_1$ (H)→(L) 37%	797.9	1.55	1.50	$S_1 \rightarrow S_0$ (H)→(L) 49%	6.41
	794.5[a]	1.70	$S_0 \rightarrow S_1$ (H)→(L) 49%					
N-MI	767.3	1.56	$S_0 \rightarrow S_1$ (H)→(L) 35%	817.0	1.52	1.59	$S_1 \rightarrow S_0$ (H)→(L) 49%	6.29
	833.8[a]	1.77	$S_0 \rightarrow S_1$ (H)→(L) 38%					
N-MIF	766.6	1.55	$S_0 \rightarrow S_1$ (H)→(L) 35%	815.4	1.52	1.56	$S_1 \rightarrow S_0$ (H)→(L) 49%	6.41
	836.2[a]	1.75	$S_0 \rightarrow S_1$ (H)→(L) 38%					
N-MICF	775.3	1.57	$S_0 \rightarrow S_1$ (H)→(L) 35%	822.9	1.51	1.55	$S_1 \rightarrow S_0$ (H)→(L) 48%	6.53
	842.0[a]	1.79	$S_0 \rightarrow S_1$ (H)→(L) 38%					
N-MIN	737.8	1.39	$S_0 \rightarrow S_1$ (H)→(L) 37%	779.7	1.59	1.47	$S_1 \rightarrow S_0$ (H)→(L) 49%	6.21
	798.9[a]	1.58	$S_0 \rightarrow S_1$ (H)→(L) 39%					

[a]In chloroform. [b]Experimental data.[18c,19a] [c]In tetrahydrofuran.

was considered by using the PCM approach, the λ^{O}_{max} values of all molecules were calculated in chloroform solution except for molecule **N-QRN** in tetrahydrofuran for the purpose of accordance with the experiment condition.[18c] The calculated data of chromophores **N-QR**, **DI**, and **N-QRN** in solvent are 698.6, 752.0, and 680.2 nm, which match well with the experimental results (685, 760, and 673 nm), respectively.[18c,19a]

As clearly shown in Table 3, all chromophores display an intense absorption in the near-infrared region in the solution. The absorption peaks with the largest oscillator strength for all molecules are assigned to $\pi-\pi^*$ character, arising from $S_0 \rightarrow S_1$, HOMO→LUMO main transition. To gain insight into the intermolecular charge transfer, the frontier molecular orbitals (FMO) containing the highest HOMO and lowest LUMO are illustrated in Figure 3. Interestingly, it can be found that the electronic densities of HOMO and LUMO are located at the center for the symmetrical molecules. The behavior of the electronic density distribution suggests that the $\pi-\pi^*$ transitions occur. However, for the unsymmetrical molecules, the charge transfer clearly takes place from the terminal groups to the center for the HOMO→LUMO transition. As a result, the series of N-MI molecules display the lower energy gaps. Chemical modifications of **Center** result in considerable bathochromic shifts of the absorption band and the enhancement of the oscillator strength, indicative of the substantial interactions between the *N*-annulated quaterrylene center and terminal groups. Increasing the conjugated length induces a significant bathochromic shift of the absorption band, which is just corresponding to the $\Delta E_{H\text{-}L}$ above. It is noteworthy that the λ^{O}_{max} values are bathochromically shifted in the order 742.9 nm (**N-QRNPh**) < 752.0 nm (**DI**) < 794.5 nm (**NMI-2N**) when replacing the terminal groups with imide moieties. By increasing the strength of the electron-donating terminal groups, the λ^{O}_{max} values exhibit red-shifts, that is, **Center** (670.3 nm) < **N-QRN** (680.2 nm) < **N-QRT** (687.4 nm) < **N-QR** (698.6 nm) < **N-QRNPh** (742.9 nm). The introduction of dicarboximides to the *N*-annulated quaterrylene center leads to significant red-shifts by 80 nm (**Center** < **Center11**) and 65 nm (**N-QRT** < **DI**), respectively. As incorporating different electron-withdrawing or -donating groups in molecule **Center11**, the λ^{O}_{max} values exhibit very slight red-shifts, such as **Center11** (750.5 nm) < **DI** (752.0 nm) < **DI-NS** (756.3 nm). This implies that the maximum OPA spectra are almost determined by the *N*-annulated quaterrylene dicarboximide center. The conclusion is consistent with our previous reports.[14] The asymmetry molecules exhibit more pronounced red-shifts of the absorption

dx.doi.org/10.1021/jo202154h | J. Org. Chem. 2012, 77, 585–597

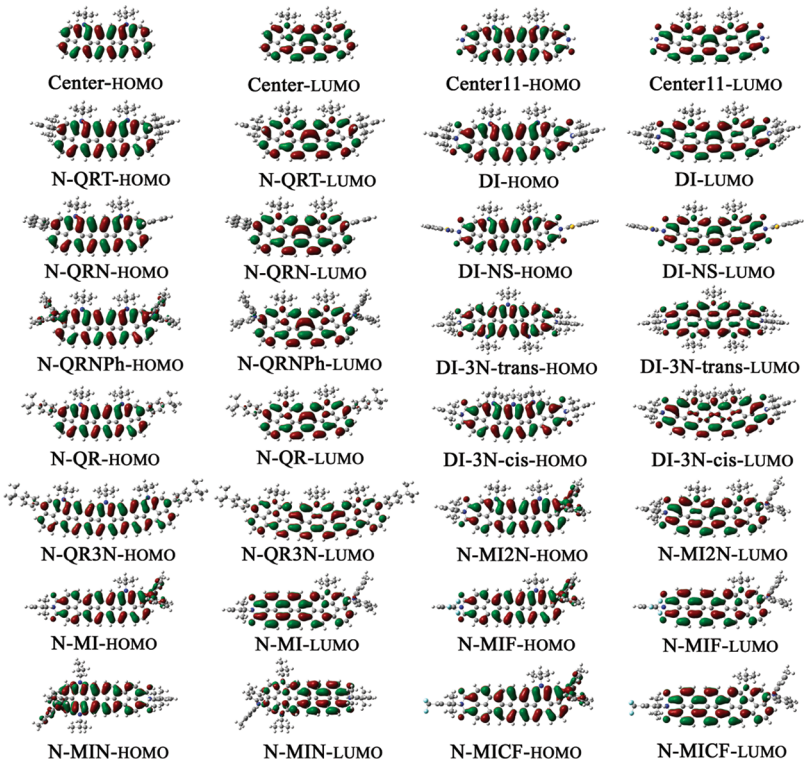

Figure 3. Contour surfaces of the HOMO and LUMO orbitals for all of the molecules studied.

band with respect to the symmetry ones, such as, **N-MI2N** > **N-QRNPh**, and **N-MI2N** > **DI**. On the other hand, reducing one *N*-annulated bridge on the long or short axis at the bay position of the compounds further leads to distinct red-shifts of the absorption band, such as 794.5 nm (**N-MI2N**) < 833.8 nm (**N-MI**), 798.9 nm (**N-MIN**) < 833.8 nm (**N-MI**), and 689.9 nm (**DI-3N-cis**) < 728.6 nm (**DI-3N-trans**) < 752.0 nm (**DI**). Moreover, it can be also found that the λ^{O}_{max} of *trans*-isomer is bathochromically shifted by 30 nm as compared to the *cis*-isomer. Incorporating fluorine atoms in the terminal group and substituting at different positions in molecule **N-MI** produce a little change of λ^{O}_{max}, with the largest red-shift of 8 nm. Additionally, the extension of the conjugated framework along the long molecular axis induces not only a drastically bathochromic shift but also a strong enhancement of its intensity. For example, the λ^{O}_{max} of molecule **N-QR3N** is red-shifted by 203 nm relative to that of **N-QR**. The oscillator strength enhances from 1.71 for **N-QR** to 2.77 for **N-QR3N**. This demonstrates that the ladder-type conjugated structure leads to a great degree of planarity and corresponding large delocalization of electron wave functions.[9]

The calculated emission spectra for chromophores **N-QR**, **DI**, and **N-QRN** in gas are 738.2, 774.8, and 724.6 nm, respectively. These results appear to be in reasonable agreement with the experiment data 700, 775, and 694 nm, respectively. The strongest emission peaks with the largest oscillator strength are all assigned to the $\pi-\pi^*$ type, arising from the S_1. All the transitions are caused from HOMO to LUMO. The Stoke's shift between the absorption and emission band ranges from 10 to 50 nm. The small Stoke's shift is probably ascribed to the central core skeleton with the rigid structure. All chromophores display intense absorption and emission peaks in the near-infrared region, which implies that they can be used as NIR absorption and emission materials. As in the case of the absorption spectra, the emission wavelengths exhibit the similar changing trends. By replacing the di-p-tolylamino substituent with the imide and 2,6-diisopropylphenyl moieties at the terminal, the λ^{E}_{max} values are bathochromically shifted with the trend of **N-QRNPh** (785.2 nm), **DI** (774.8 nm), **NMI-2N** (797.9 nm). Increasing the strength of the electron-donating terminal group, the λ^{E}_{max} values exhibit red-shifts, that is, **Center** (702.2 nm) < **N-QRN** (724.6 nm) < **N-QRT** (725.3 nm) < **N-QR** (738.2 nm) < **N-QRNPh** (785.2 nm). The introduction of dicarboximides to the *N*-annulated quaterrylene center leads to large red-shifts by 59 nm (**Center** < **Center11**) and 50 nm (**N-QRT** < **DI**), respectively. The modification of molecule **Center11** induces a slight red-shift of the emission spectra, such as **Center11** (760.8 nm) < **DI-NS** (772.7 nm) < **DI** (774.8 nm). This implies that the maximum emission spectra of the *N*-annulated quaterrylene dicarboximide derivatives are also dependent on the central core. The asymmetry molecules exhibit significantly red-shifted emission with respect to the symmetry ones, that is, **N-MI2N** > **N-QRNPh**, and **N-MI2N** > **DI**. On the other hand, reducing one *N*-annulated bridge on the long or short axis at the bay position of the asymmetry compounds still leads to significant red-shifts of the emission band, such as 797.9 nm (**N-MI2N**) < 817.0 nm (**N-MI**), 779.7 nm (**N-MIN**) < 817.0 nm (**N-MI**), and 708.7 nm (**DI-3N-cis**) < 744.1 nm (**DI-3N-trans**) < 774.8 nm (**DI**). Incorporating fluorine atoms in the terminal group and substituting at different positions in molecule **N-MI** produce a little change of the emission band, with the largest deviation of 6 nm. Additionally, extending the conjugation length induces a remarkable red-shift of NIR emission. For example, the λ^{E}_{max} of molecule **N-QR3N** is red-shifted by 191 nm relative to **N-QR**. This suggests that the ladder-type conjugated structure produces a great degree of planarity and corresponding large electron-delocalization.

Table 3 also lists the emission lifetimes (τ) calculated for spontaneous emission by using the Einstein transition

dx.doi.org/10.1021/jo202154h | *J. Org. Chem.* 2012, 77, 585–597

Table 4. One- and Two-Photon Absorption Properties (ZINDO)

molecule	λ^{O}_{max}/nm	f	transition nature	λ^{T}_{max}/nm	δ_{max}/GM	transition channel and nature
Center	654.1	0.89	$S_0 \rightarrow S_1$ (H)→(L) 83%	752.3	7482.6	$S_0 \rightarrow S_1 \rightarrow S_{23}$ (H, H)→(L, L) 14%
	659.5[a]	0.88[a]	$S_0 \rightarrow S_1$ (H)→(L) 83%			(H-1)→(L+4)13%
				755.1[a]	7503.1[a]	$S_0 \rightarrow S_1 \rightarrow S_{23}$ (H, H)→(L, L) 13%
						(H-1)→(L+4) 13%
Center11	727.4	1.14	$S_0 \rightarrow S_1$ (H)→(L) 82%	841.1	11076.5	$S_0 \rightarrow S_1 \rightarrow S_{24}$ (H-1)→(L+2) 12%
	788.0[a]	1.22[a]	$S_0 \rightarrow S_1$ (H)→(L) 79%			(H-9)→(L) 11%
				880.6[a]	11976.6[a]	$S_0 \rightarrow S_1 \rightarrow S_{22}$ (H, H)→(L, L) 14%
						(H-1)→(L+2) 13%
						(H-9)→(L) 11%
N-QRNPh	703.0	1.11	$S_0 \rightarrow S_1$ (H)→(L) 83%	821.1	9470.4	$S_0 \rightarrow S_1 \rightarrow S_{27}$ (H-1)→(L+9) 18%
	708.6[a]	1.09[a]	$S_0 \rightarrow S_1$ (H)→(L) 83%			(H-2)→(L+8) 17%
				824.4[a]	9076.5[a]	$S_0 \rightarrow S_1 \rightarrow S_{27}$ (H-1)→(L+9) 18%
						(H-2)→(L+8) 17%
N-QR	674.4	1.12	$S_0 \rightarrow S_1$ (H)→(L) 83%	777.8	12579.3	$S_0 \rightarrow S_1 \rightarrow S_{25}$ (H, H)→(L, L) 13%
	679.2[a]	1.10[a]	$S_0 \rightarrow S_1$ (H)→(L) 84%	780.8[a]	12550.5[a]	$S_0 \rightarrow S_1 \rightarrow S_{25}$ (H, H)→(L, L) 12%
N-QRT	680.3	1.03	$S_0 \rightarrow S_1$ (H)→(L) 84%	786.7	8865.3	$S_0 \rightarrow S_1 \rightarrow S_{25}$ (H)→(L) 11%
	680.5[a]	1.02[a]	$S_0 \rightarrow S_1$ (H)→(L) 84%			(H-1)→(L+5) 11%
				783.7[a]	10184.6[a]	$S_0 \rightarrow S_1 \rightarrow S_{25}$ (H, H)→(L, L) 14%
N-QRN	653.8	1.11	$S_0 \rightarrow S_1$ (H)→(L) 82%	777.8	10659.5	$S_0 \rightarrow S_1 \rightarrow S_{31}$ (H, H)→(L, L) 22%
	661.6[a]	1.10[a]	$S_0 \rightarrow S_1$ (H)→(L) 82%	783.7[a]	10861.8[a]	$S_0 \rightarrow S_1 \rightarrow S_{30}$ (H, H)→(L, L) 18%
N-QR3N	756.9	1.83	$S_0 \rightarrow S_1$ (H)→(L) 78%	858.6	47842.6	$S_0 \rightarrow S_1 \rightarrow S_{32}$ (H, H)→(L, L) 14%
	761.3[a]	1.81[a]	$S_0 \rightarrow S_1$ (H)→(L) 78%	862.2[a]	47286.8[a]	$S_0 \rightarrow S_1 \rightarrow S_{32}$ (H, H)→(L, L) 12%
DI	768.3	1.19	$S_0 \rightarrow S_1$ (H)→(L) 80%	907.3	2354.1	$S_0 \rightarrow S_1 \rightarrow S_{29}$ (H)→(L+9) 18%
	800.3[a]	1.35[a]	$S_0 \rightarrow S_1$ (H)→(L) 78%	895.8[a]	10371.2[a]	$S_0 \rightarrow S_1 \rightarrow S_{27}$ (H, H)→(L, L) 14%
DI-NS	772.6	1.22	$S_0 \rightarrow S_1$ (H)→(L) 80%	895.8	2575.4	$S_0 \rightarrow S_1 \rightarrow S_{23}$ (H)→(L+9) 18%
	804.1[a]	1.39[a]	$S_0 \rightarrow S_1$ (H)→(L) 78%	907.7[a]	9882.6[a]	$S_0 \rightarrow S_1 \rightarrow S_{23}$ (H-3)→(L+8) 17%
DI-3N-trans	774.9	1.14	$S_0 \rightarrow S_1$ (H)→(L) 80%	899.7	2487.8	$S_0 \rightarrow S_1 \rightarrow S_{29}$ (H-13)→(L) 13%
	817.2[a]	1.33[a]	$S_0 \rightarrow S_1$ (H)→(L) 79%	958.2[a]	5719.3[a]	$S_0 \rightarrow S_1 \rightarrow S_{19}$ (H)→(L+10) 22%
DI-3N-cis	784.4	1.11	$S_0 \rightarrow S_1$ (H)→(L) 80%	919.8	1330.6	$S_0 \rightarrow S_1 \rightarrow S_{25}$ (H)→(L+6) 13%
	846.8[a]	1.10[a]	$S_0 \rightarrow S_1$ (H)→(L) 74%	995.1[a]	885.0[a]	$S_0 \rightarrow S_1 \rightarrow S_{16}$ (H-10)→(L) 23%
N-MI2N	781.6	1.11	$S_0 \rightarrow S_1$ (H)→(L) 78%	862.2	6025.3	$S_0 \rightarrow S_1 \rightarrow S_{26}$ (H-4)→(L+1) 13%
	822.3[a]	1.10[a]	$S_0 \rightarrow S_1$ (H)→(L) 73%	911.7[a]	5962.3[a]	$S_0 \rightarrow S_1 \rightarrow S_{18}$ (H)→(L+6) 15%
N-MI	782.2	1.12	$S_0 \rightarrow S_1$ (H)→(L) 78%	876.8	6133.4	$S_0 \rightarrow S_1 \rightarrow S_{26}$ (H-4)→(L+1) 12%
	812.8[a]	1.13[a]	$S_0 \rightarrow S_1$ (H)→(L) 75%			(H-12)→(L+2) 11%
				899.7[a]	7578.3[a]	$S_0 \rightarrow S_1 \rightarrow S_{24}$ (H-11)→(L+2) 11%
N-MIF	765.4	1.08	$S_0 \rightarrow S_1$ (H)→(L) 78%	841.1	16752.3	$S_0 \rightarrow S_1 \rightarrow S_{26}$ (H-13)→(L) 12%
	825.4[a]	1.14[a]	$S_0 \rightarrow S_1$ (H)→(L) 74%	923.9[a]	5940.6[a]	$S_0 \rightarrow S_1 \rightarrow S_{23}$ (H-10)→(L+2) 13%
N-MICF	797.0	1.12	$S_0 \rightarrow S_1$ (H)→(L) 77%	895.8	4501.6	$S_0 \rightarrow S_1 \rightarrow S_{25}$ (H-3)→(L+1) 15%
	818.7[a]	1.13[a]	$S_0 \rightarrow S_1$ (H)→(L) 75%			(H-12)→(L+2) 15%
				911.7[a]	6876.0[a]	$S_0 \rightarrow S_1 \rightarrow S_{24}$ (H-11)→(L+2) 11%
N-MIN	778.9	1.00	$S_0 \rightarrow S_1$ (H)→(L) 75%	884.3	2825.6	$S_0 \rightarrow S_1 \rightarrow S_{26}$ (H-12)→(L+2) 15%
	828.4[a]	1.03[a]	$S_0 \rightarrow S_1$ (H)→(L) 72%	932.2[a]	2798.9[a]	$S_0 \rightarrow S_1 \rightarrow S_{19}$ (H-10)→(L) 11%

[a]In chloroform.

probabilities according to the formula (in au):[34,35]

$$\tau = \frac{c^3}{2(E_{Flu})^2 f} \quad (3)$$

Where c is the velocity of light, E_{Flu} is the transition energy, and f is the oscillator strength. The data of E_{Flu} and f are also shown in Table 3. The calculated emission lifetimes of all molecules are in the same order of magnitude (ranging from 4.90 to 7.09 ns). Thus, the emission lifetimes for the *N*-annulated quaterrylene derivatives are lower than that of **Center**. The molecules bearing the imide groups or longer π-conjugated system exhibit stronger emission and shorter emission lifetimes, respectively.

In order to accurately predict one-photon absorption properties, the ZINDO program was also employed including double electronic excitation. For all of the molecules, the CI-active spaces were restricted to the 31 highest-occupied and 31 lowest-unoccupied π orbitals for the singly excited configuration and 3 highest occupied and 3 lowest unoccupied π orbitals for the doubly excited configuration. The ZINDO method which is both reliable and efficient to predict the vertical excitation energy of the *X*-annulated rylenes has been previously reported by Shuai group.[36] Most importantly, it can be applied to large molecules, which offers us an efficient tool for designing TPA materials in this contribution. As observed in Table 4, the λ^{O}_{max} values of **N-QR**, **DI** and **N-QRN** are 674.4, 768.3, and 653.8 nm obtained by ZINDO/SDCI, which are consistent with the experiment data 685, 760, and 673 nm, respectively. At this point, it has to be noted that the ZINDO method predicts the almost similar changing trends above to TD-DFT//B3LYP/6-31G*, except for the opposite order 784.4 nm (**DI-3N-cis**) > 774.9 nm (**DI-3N-trans**) > 768.3 nm

dx.doi.org/10.1021/jo202154h | J. Org. Chem. 2012, 77, 585–597

(**DI**). This is ascribed to the systematic error from the different methods. The configuration weights analysis of the ground and excited states for all molecules indicates that the lowest and strongest absorption band ($S_0 \rightarrow S_1$) is exclusively composed of the HOMO→LUMO electronic excitation. This is also in accordance with the transition assignment of the B3LYP functional. The good result makes us confident that the computed TPA properties in the following discussion should be reliable. When the solvent influence was considered on the OPA properties, ZINDO calculations by PCM were carried out for all of the molecules. As seen in Table 4, the OPA spectra of the molecules bearing the *N*-annulated rylene skeleton batho-chromically shift by at most 7.8 nm in chloroform solution with respect to those in gas. For instance, the OPA absorption band of molecule **N-QR3N** in solvent (761.3 nm) is slightly larger by 4.4 nm than that in gas (756.9 nm). So it is concluded that the solvent influence on the optical properties for the series of NQR molecules is very slight and could be ignored on some extent. In contrast, it should be stressed that a solvatochromism effect on the OPA spectra is observed for the series of DI and N-MI molecules with imide moieties in the central core. The λ^{O}_{max} values in gas are red-shifted by 21.7−62.4 nm with respect to those in chloroform solution. This solvent effect is due to the fact that the carboximide substitution possesses high electron affinity and thus increases the intramolecular charge transfer in polar solvent. In general, the absorption spectra of the two series of DI and N-MI molecules show a clear solvent dependence.

4. Two-Photon Absorption Properties. The well-defined two-photon absorption spectra were determined over a broad spectral range by utilizing ZINDO, and the calculated results were shown in Figure 4. The detailed data containing maximum TPA wavelength (λ^{T}_{max}), maximum TPA cross

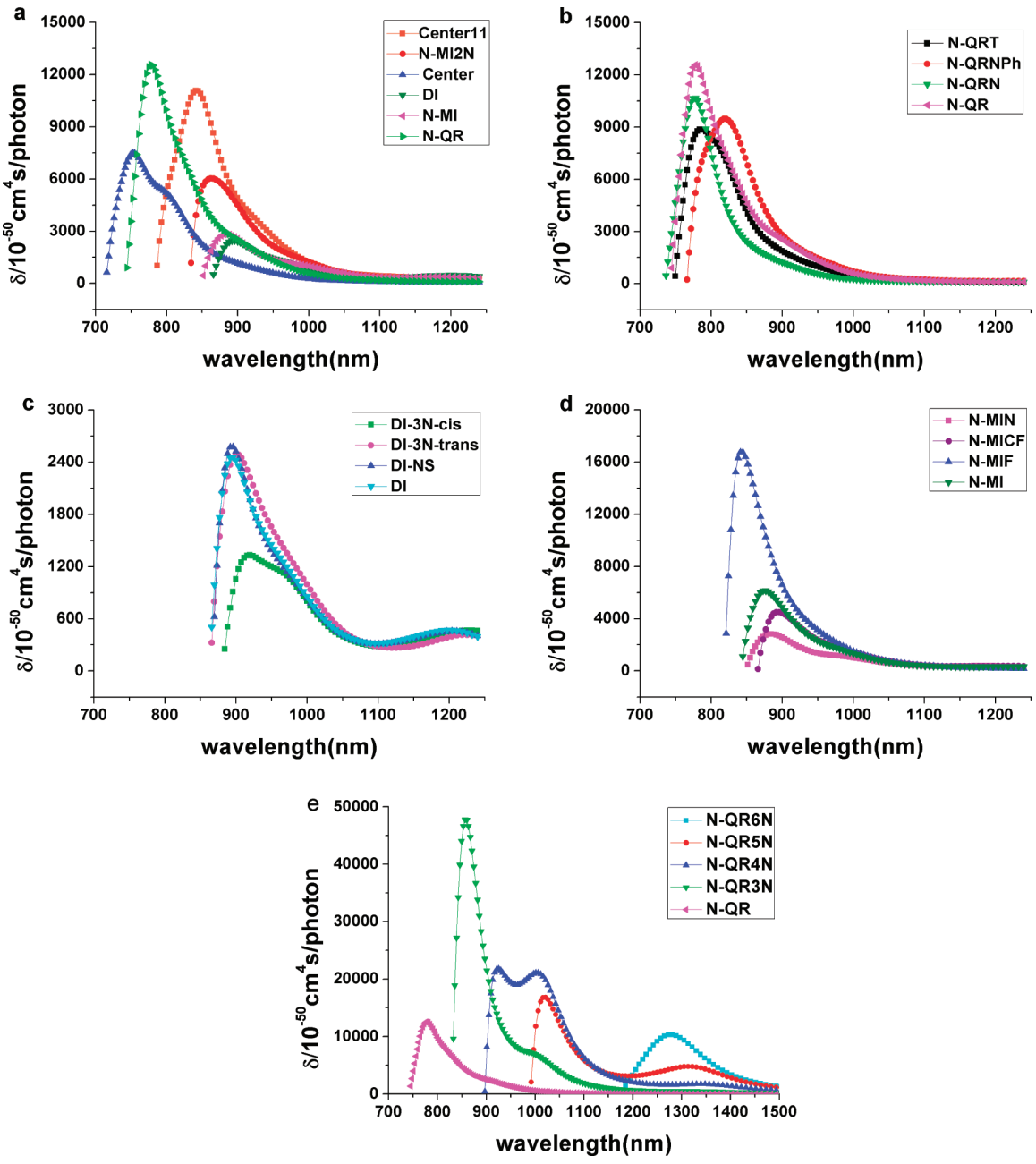

Figure 4. Two-photon absorption spectra for all of the molecules in gas.

dx.doi.org/10.1021/jo202154h | *J. Org. Chem.* 2012, 77, 585−597

section (δ_{max}), and transition nature are all listed in Table 4. As observed in Figure 4 and Table 4, all chromophores exhibit the intense two-photon absorption in NIR region with corresponding TPA cross sections $\delta_{max} \approx 2300-48000$ GM. This shows that they can be suitable for the application in two-photon fluorescence labeling. The later sections are devoted to discussing some structural and other aspects that can affect the TPA properties.

4.1. Effects of Terminal Groups and Central Core. It can be seen from Figures 4a and 4b and Table 4 that the δ_{max} values increase by 1000 GM with the introduction of electron-donating groups into molecule **Center**, that is, **Center** (7482.6 GM) < **N-QRT** (8865.3 GM) < **N-QRNPh** (9470.4 GM) < **N-QRN** (10659.5 GM) < **N-QR** (12579.3 GM), following the definite red-shift of the TPA spectra. From Figure 4c, molecule **DI-NS** exhibits the little larger TPA cross section than **DI**, indicating that the benzothiazole-substituted terminal groups increase the π-electron polarization. As shown in Figure 4d, incorporating fluorine atoms in the terminal group and substituting at the different positions in molecule **N-MI** produce hypsochromic shifts of the λ^{T}_{max}, and the δ_{max} increase in the order of **N-MICF** (4501.6 GM), **N-MI** (6133.4 GM) and **N-MIF** (16752.3 GM). Remarkably, the δ_{max} value of molecule **N-MIF** is around 3-fold greater than that of **N-MI**. By replacing the di-p-tolylamino substituent of **N-QRNPh** with the imide and 2,6-diisopropylphenyl moieties at the terminal end, the TPA cross section decreases in the order **N-QRNPh** > **N-MI2N** > **DI**. In order to get a better understanding of intramolecular charge transfer (ICT) in the TPA transition, we calculated the net charge change ($|\Delta Q|$, $\Delta Q = Q_n - Q_0$, Q_0 and Q_n denote the Mulliken charge of the ground state and the final state, respectively) of the three molecules. The net charge changes by performing on the central core are 0.26555, 0.09401, and 0.02662 e for **N-QRNPh**, **N-MI2N**, and **DI**, respectively. This suggests that the *N*-annulated quaterrylene molecule can efficiently transfer intramolecular charge and in turn enhances δ_{max} relative to its imide derivatives. As shown in Figure 4a, it can be observed that the δ_{max} value of molecule **Center11** bearing dicarboximide groups increase by 3593.9 GM, but the TPA spectra are red-shifted by 100 nm with respect to its quaterrylene **Center**.

4.2. Effect of N-annulated Bridge. By adding one *N*-annulated bridge at the bay position on the long axis, molecule **DI-3N-cis** exhibits smaller δ_{max} (1330.6 GM) at 919.8 nm than **DI** (2354.1 GM) at 907.3 nm. The λ^{T}_{max} value of **DI-3N-trans** remains unchanged and its δ_{max} value is increased by 133.7 GM as compared to **DI** (Figure 4c). The δ_{max} of *trans*-isomer is larger by 1157.2 GM than that of the *cis*-isomer, which may be attributed to the *trans*-isomer can facilitate the charge transfer. As shown in Table 4 and Figure 4a, it can be noted that adding one *N*-annulated bridge on molecule **N-MI** leads to the decrease of δ_{max} (**N-MI2N**). In contrast with adding one *N*-annulated bridge on the short axis, the δ_{max} value for **N-MIN** is 2825.6 GM at 884.3 nm, which decreases by 3307.8 GM relative to **N-MI** at 876.8 nm. Generally, adding one *N*-annulated bridge at the bay position on both the long and short axis results in the decrease of δ_{max}.

4.3. Effect of Conjugation Length. From Figure 4e, it can be observed that increasing the π-conjugated length induces a marked bathochromic shift of the TPA absorption band and enhancement of the TPA cross section. For example, the λ^{T}_{max} of **N-QR3N** is red-shifted by 80.8 nm relative to **N-QR**. Noteworthily, the δ_{max} value of molecule **N-QR3N** (47842.6 GM) is 3.8 times as large as **N-QR** (12579.3 GM). In order to further investigate the influence of the extension of the conjugated framework on the TPA properties, molecules **N-QR4N**, **N-QR5N**, **N-QR6N** (cf., Supporting Information, Figure S1) were constructed by sequentially elongating one *N*-annulated perylene unit based on molecule **N-QR3N**. The two-photon absorption spectra were determined over a broad spectral range (700−1600 nm) by using ZINDO, and the results were shown in Figure 4e. The detailed results containing OPA spectra, maximum TPA wavelength, maximum TPA cross section and transition channels are all collected (cf., Supporting Information, Table S1). From Table S1 and Figure 4e, it should be mentioned that the maximum OPA and TPA spectra are shifted to longer wavelength (λ^{O}_{max} = 674.4−935.5 nm, λ^{T}_{max} = 780.8−1280.8 nm) as the number of the *N*-annulated perylene units increases. However, it is surprising that the δ_{max} values of molecules **N-QR4N**, **N-QR5N**, and **N-QR6N** gradually decrease as the conjugation extending increases compared to molecule **N-QR3N**. This is the first time to report that enlarging the conjugation length produces the decrease of δ_{max}. For the explanation of the changing trend, the net charge change, and the bond-length alternation (BLA) parameters of these *N*-annulated rylene molecules **N-QR**, **N-QR3N**, **N-QR4N**, **N-QR5N**, and **N-QR6N** were calculated. Sum and average lengths of single C−C bonds (S-bond) and double C═C bonds (D-bond) in the π-conjugated central skeleton, BLA, Q_0, Q_n, and ΔQ are all listed in Table 5. The results show

Table 5. BLA and Net Charge Change and Related Parameters of the Series of N-QR Molecules

parameter	N-QR	N-QR3N	N-QR4N	N-QR5N	N-QR6N
sum of S-bond/Å	42.7443	65.5320	88.3078	111.0728	133.8467
av of S-bond/Å	1.4248	1.4246	1.4243	1.4240	1.4239
sum of D-bond/Å	28.0535	42.1348	56.2280	70.3240	84.4226
av of D-bond/Å	1.4027	1.4045	1.4057	1.4065	1.4070
BLA/Å	0.0221	0.0201	0.0186	0.0175	0.0169
Q_0/e	−0.2543	−0.3776	−0.5035	−0.6270	−0.7492
Q_n/e	−0.2650	−0.4008	−0.5132	−0.6339	−0.7497
$\|\Delta Q\|$/e	0.0107	0.0232	0.0097	0.0069	0.0005

that the average of S-bond decreases and the average of D-bond increases with the number of the *N*-annulated perylene units increasing. As a consequence, the BLA values decrease in the order of **N-QR** (0.0221 Å), **N-QR3N** (0.0201 Å), **N-QR4N** (0.0186 Å), **N-QR5N** (0.0175 Å), and **N-QR6N** (0.0169 Å). This indicates that the π-conjugation effect of the central skeleton extends with increasing the *N*-annulated perylene units. So the absorption band is red-shifted. However, the extension of the π-conjugation length does not always promote an enhancement of the TPA cross section. This may be attributed to the ICT. So we calculated the charge change value upon the TPA. As shown in Table 5, the maximum TPA causes the net charge change of 0.0107 e for **N-QR**, and 0.0232 e for **N-QR3N**. This indicates that ICT does enhance from **N-QR** to **N-QR3N** and accordingly results in the dramatic increase of δ_{max} for **N-QR3N**, but for molecules **N-QR4N**, **N-QR5N**, and **N-QR6N**, the net charge change decreases upon the TPA with respect to **N-QR3N** (Table 5) and thus produces a decrease of their δ_{max} values. Consequently, the changing trends of ΔQ can interpret the origin of changing rules of their TPA cross section. The results indicate that the terminal groups put their maximum polarization ability to good use in such a conjugated length for

dx.doi.org/10.1021/jo202154h | J. Org. Chem. 2012, 77, 585−597

N-QR3N. If one more unit is increased based on **N-QR3N**, the two terminal groups will exert part effect of polarization and in turn lead to the decrease of δ_{max}. Overall, increasing the number of the *N*-annulated perylene units induces a better conjugated effect and thereby a bathochromic shift of the TPA spectra to the near-infrared region. However, it results in the enhancement of δ_{max} in the certain conjugation extension range, and this conjugation extension range will depend on the polarization ability of the terminal groups. In a word, the quantity of the ICT in the TPA process should be the intrinsic essential factor in determining TPA cross section value, that is to say, enlargement of the π-system does not always enhance the TPA cross section.

4.4. Effect of Solvent. Since a proper account of the solvent effect is crucial for a direct comparison between experiment and calculation, we performed calculations on the TPA properties in chloroform solution. As shown in Table 4, the λ^{T}_{max}, δ_{max}, and transition nature in chloroform solution for the series of N-QR molecules are quite similar in gas phase. The largest deviation is made for molecule **N-QRT**, showing its TPA cross section in solvent (10184.6 GM) is 15% larger than that in gas (8865.3 GM), but the TPA spectra of the series of DI and N-MI molecules show a clearer solvent dependence, with the deviation from 11.5 to 82.8 nm. It is worthwhile noting that the δ_{max} values of molecules **N-MI2N** and **N-MIN** in gas (6025.3, 2825.6 GM) are slightly larger than those in chloroform (5962.3, 2798.9 GM), but their λ^{T}_{max} values in chloroform are longer by about 50 nm than that in gas phase. The red-shifts of λ^{T}_{max} are consistent with the ICT character of their excited states. For instance, the final TPA state of molecule **N-MI2N** is located in the lower energy region in chloroform (S_{18}) compared to that in gas (S_{26}), and the red-shifts can be also explained by their higher stabilization in solvent. The δ_{max} values of molecules **N-MI** and **N-MICF** in chloroform increase 24% and 53% as compared to those in gas, respectively. In particular, the δ_{max} values of the DI series and molecule **N-MIF** in solution do show a clear difference from those in gas, namely, molecules **DI** and **DI-NS** have shown intense TPA response with extremely high δ_{max} values of 10371.2 and 9882.6 GM in chloroform, which is about four times as great as those in gas, respectively. The δ_{max} value of molecule **DI-3N-trans** in chloroform is about 2 times higher than that in gas. The higher TPA activity in solvent can be attributed to an increased intramolecular charge transfer and a larger transition dipole moment. In contrast, it should be stressed that the δ_{max} value for molecule **N-MIF** decreases from 16752.3 GM in gas to 5940.6 GM in chloroform, which is about 3-fold smaller. Such a reduction is unprecedented. This may be related that the two *ortho* CF_3 groups featuring the strong electron affinity induce electrostatic repulsion with the nonpolar solvent and thus decrease ICT in solvent.

In general, the solvent plays a crucial role on the TPA properties of the two series of DI and N-MI molecules. Therefore, this leads to some changing trends that are different from those in vacuum. It can be observed from Table 4 that the δ_{max} values in chloroform increase in the order of **Center** (7503.1 GM), **N-QRNPh** (9076.5 GM), **N-QRT** (10184.6 GM), **N-QRN** (10861.8 GM), and **N-QR** (1255.5 GM), with the introduction of electron-donating groups into molecule **Center**, which shows a smaller change relative to those above discussion in gas. The δ_{max} values of both **Center11** and **DI** bearing dicarboximide groups in solvent increase by 4473.5 and 186.6 GM, following the significantly red-shifted TPA spectra as compared to their corresponding *N*-annulated quaterrylenes **Center** and **N-QRT**, respectively. The relative changing rules appear with some differences from those in vacuum. Replacing the 2,6-diisopropylphenyl moieties with electron-withdrawing benzothiazole-substituted terminal groups and adding the *N*-annulated bridge at different positions in molecule **DI** produces hypsochromic shifts of λ^{T}_{max} and the δ_{max} decreases in the order of **DI** (10371.2 GM at 895.8 nm), **DI-NS** (9882.6 GM at 907.7 nm), **DI-3N-trans** (5719.3 GM at 958.2 nm), and **DI-3N-cis** (885.0 GM at 995.1 nm). From the changing rules, we observed that molecule **DI-NS** exhibits a slightly smaller TPA cross section than **DI**, which is different from the change in gas phase. This difference should be a consequence of the solvent effect. Moreover, adding one *N*-annulated bridge at the bay position on the long axis leads to the decrease of δ_{max}. The δ_{max} for molecule **DI-3N-trans** turns out to be about one-half of **DI**. The decrease is also made for molecules of **N-MI2N** and **N-MI**. For instance, molecule **N-MI2N** exhibits smaller δ_{max} (5962.3 GM) at 911.7 nm than **N-MI** (7578.3 GM) at 899.7 nm. In contrast, by adding one *N*-annulated bridge on the short axis, the δ_{max} value for **N-MIN** is 2798.9 GM at 932.2 nm, which decreases by 4779.4 GM with respect to **N-MI** at 899.7 nm. From the analysis above, it can be concluded that adding one *N*-annulated bridge at the bay position both on the long and short axis leads to the reduction of δ_{max} and the red-shift of λ^{T}_{max}. From Table 4, it can be found that the *N*-annulated quaterrylene diimide molecule exhibits large δ_{max} in comparison with *N*-annulated quaterrylene and *N*-annulated perylene-perylene imide molecules, that is, **DI** > **N-QRNPh** > **N-MI2N**. This demonstrates that the *N*-annulated quaterrylene diimide molecule can efficiently transfer intramolecular charge in chloroform and thus enhances TPA cross sections. As shown, incorporating fluorine atoms in the terminal group and substituting at different positions in molecule **N-MI** produce bathochromic shifts of the λ^{T}_{max} and the δ_{max} decrease in the order **N-MI** (7578.3 GM at 899.7 nm) > **N-MICF** (6876.0 GM at 911.7 nm) > **N-MIF** (5940.6 GM at 923.9 nm). In sum, incorporating the different terminal groups and increasing the π-conjugated length make the enhancement of δ_{max} on some extent, and adding the number of *N*-annulated bridges induces the red-shifts of λ^{T}_{max} and decrease of δ_{max}.

Generally, the position and relative strength of the two-photon resonance could be estimated with the following three-level energy model form of the SOS expression:[27,28,37]

$$\delta \propto \frac{M_{0k}^2 M_{kn}^2}{(E_{0k} - E_{0n}/2)^2 \Gamma} + \frac{M_{0n}^2 \Delta\mu_{0n}^2}{(E_{0n}/2)^2 \Gamma} \quad (4)$$

Here, M_{ij} is the transition dipole moment from the state i to j,; E_i is the corresponding excitation energy, and the subscripts 0, k, and n refer to the ground state S_0, the intermediate state S_k, and the TPA final state S_n, respectively; $\Delta\mu_{0n}$ is the state dipole moment difference between S_0 and S_n; the damping factor Γ here is set to 0.14 eV. A simplified form becomes the following formula:

$$\delta \propto \frac{M_{0k}^2 M_{kn}^2}{(E_{0k} - E_{0n}/2)^2 \Gamma} \quad (5)$$

On the basis of the theory, the transition dipole moments between the ground state and charge transfer state, and the energy levels in the TPA process are schemed in Figure 5. We can observe that introducing the strength of electron-donating terminal groups and increasing the conjugated length in molecule **Center** induce to the enhancement of M_{0k}

dx.doi.org/10.1021/jo202154h | J. Org. Chem. 2012, 77, 585–597

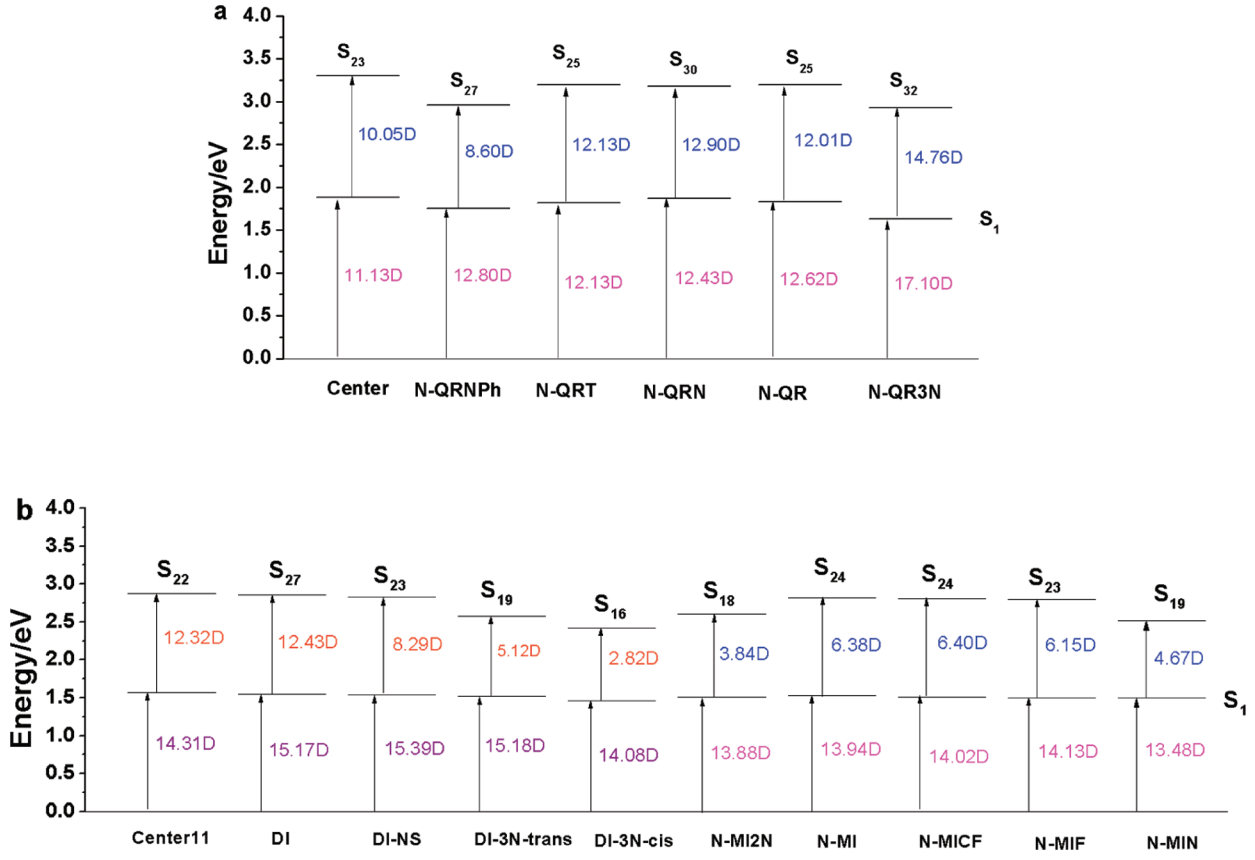

Figure 5. Scheme of ZINDO-predicted transition moments (in Debye units) and energy levels in chloroform solution.

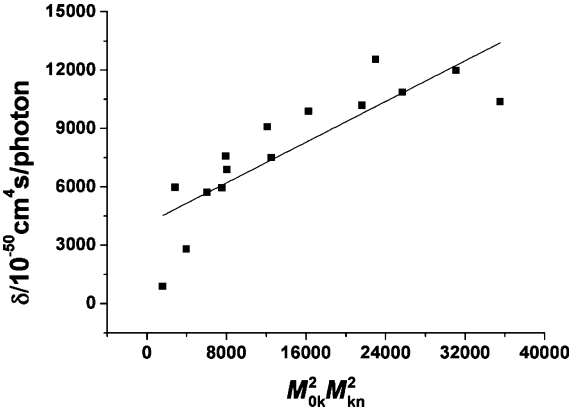

Figure 6. Plot of δ_{max} versus $M^2_{0k}M^2_{kn}$.

(the transition dipole moment between the ground state and intermediate state) and M_{kn} (the transition dipole moment between the intermediate state and final state) (Figure 5a). Remarkably, molecule **N-QR3N** exhibits the largest M_{0k} and M_{kn} among all of the molecules. Modification of molecule **Center11** including the introduction of the terminal substituents and addition of one *N*-annulated bridge at the bay position results in the decrease of M_{kn} and the increase of the energy tuning term $(E_{0k} - E_{0n}/2)$ and thus makes the TPA cross section decrease (Figure 5b). The δ_{max} values of both **N-MI2N** and **N-MIN** are smaller than that of **N-MI**, as the *N*-annulated bridge at the bay position on the long and short axis increased, which is ascribed to the reduction of M_{0k} and M_{kn}. According to the results above, it can be concluded that the transition moments play a crucial role in determining the TPA cross section. So the relationship between δ_{max} and $M^2_{0k}M^2_{kn}$ of all studied molecules except for **N-QR3N** is depicted in Figure 6. As can be seen, the calculated points are averagely distributed on the two sides of the line. Their relation is directly proportional to each other.[38] By the analysis of Figures 5 and 6, we believe that the transition dipole moment is largely responsible for the changing trends of δ_{max}.

CONCLUSIONS

In this work, the investigation of the geometric and electronic structures, as well as one-photon absorption, emission, and two-photon absorption properties, for a series of *N*-annulated quaterrylene chromophores could provide penetrated insight into the correlations between the molecular structure and the linear and nonlinear optical properties. The effects of terminal groups, the number of *N*-annulated bridges and the conjugated length as well as the solvent on OPA and TPA properties were thoroughly discussed. It should be stressed that the solvent effect on the OPA spectra calculated by TDDFT is significant relative to the calculations in vacuum. Moreover, the OPA and TPA properties of the two series of DI and N-MI molecules obtained by the ZINDO method show a clear solvent dependence, which is attributed to the carboximide chromophore possessing high electron affinity and thus increasing the intramolecular charge transfer in chloroform, but the λ^{O}_{max}, λ^{T}_{max}, and δ_{max} values in chloroform solution for the series of N-QR molecules appear quite similar in the gas phase. The calculated results show that introducing electron-donating groups into molecule **Center** leads to red-shifts of the OPA, emission and TPA spectra, lower emission lifetimes, and enhanced TPA cross sections. The *N*-annulated quaterrylenes

dx.doi.org/10.1021/jo202154h | J. Org. Chem. 2012, 77, 585–597

exhibit larger δ_{max} and shorter OPA, emission and TPA spectra than their corresponding dicarboximides. By adding one *N*-annulated bridge at the bay position both on the short and long axis, the λ^{T}_{max} values are red-shifted and the δ_{max} values decrease in chloroform. Incorporating fluorine atoms in the terminal groups and substituting at different positions in molecule **N-MI** produce the reduction of δ_{max} but the red-shift of λ^{O}_{max} in solvent. Furthermore, increasing the conjugated length induces a significant bathochromic shift of the OPA and TPA absorption bands and enhancement of δ_{max}. Remarkably, the δ_{max} value of molecule **N-QR3N** (47286.8 GM) is around 4 times greater than that of **N-QR** (12550.5 GM), but the δ_{max} value then decreases while one or more units are increased on the base of **N-QR3N**. That is to say that enlargement of the π-system does not always enhance the TPA cross section. This is the first report that enlarging the conjugation length produces a decrease of the TPA cross section. We explained the changing trends of δ_{max} by the transition moment and ICT and drew a conclusion that the quantity of the ICT in the TPA process should be the intrinsic essential factor in determining δ_{max}. Additionally, the transition dipole moment is also responsible for the changing trends of δ_{max}. Overall, all *N*-annulated quaterrylene and their imide derivatives exhibit remarkable properties, such as low energy band gap, intense NIR absorption and emission, and large TPA cross sections, which is important to two-photon fluorescent labeling materials, and these chromophores could be used to construct graphene-type nanoribbon materials. The investigation could provide penetrated insight into the structure−property relationships and will contribute to the guideline for the experimental design.

■ ASSOCIATED CONTENT

Supporting Information

Structures of molecules **N-QR4N**, **N-QR5N**, and **N-QR6N** (Figure S1); one- and two-photon absorption properties of molecules **N-QR4N**, **N-QR5N**, and **N-QR6N** (Table S1); and Cartesian coordinates of the optimized ground-state structures. This material is available free of charge via the Internet at http://pubs.acs.org.

■ AUTHOR INFORMATION

Corresponding Author

*E-mail: aimin_ren@yahoo.com.

■ ACKNOWLEDGMENTS

This work is supported by the Natural Science Foundation of China (No. 20973078 and 21173099), as well as Special Funding to Basic Scientific Research Projects for Central Collages. We also acknowledge Prof. Jishan Wu for valuable and helpful discussions.

■ REFERENCES

(1) Silly, M. G.; Porres, L.; Mongin, O.; Chollet, P. A.; Blanchard-Desce, M. *Chem. Phys. Lett.* **2003**, *379*, 74−80.

(2) (a) LaFratta, C. N.; Fourkas, J. T.; Baldacchini, T.; Farrer, R. A. *Angew. Chem., Int. Ed.* **2007**, *46*, 6238−6258. (b) Scott, T. F.; Kowalski, B. A.; Sullivan, A. C.; Bowman, C. N.; McLeod, R. R. *Science* **2009**, *324*, 913−917.

(3) Velusamy, M.; Shen, J. Y.; Lin, J. T.; Lin, Y. C.; Hsieh, C. C.; Lai, C. H.; Lai, C. W.; Ho, M. L.; Chen, Y. C.; Chou, P. T.; Hsiao, J. K. *Adv. Funct. Mater.* **2009**, *19*, 2388−2397.

(4) Feng, X. J.; Wu, P. L.; Bolze, F.; Leung, H. W. C.; Li, K. F.; Mak, N. K.; Kwong, D. W. J.; Nicoud, J.-F.; Cheah, K. W.; Wong, M. S. *Org. Lett.* **2010**, *12*, 2194−2197.

(5) Jasieniak, J. J.; Fortunati, I.; Gardin, S.; Signorini, R.; Bozio, R.; Martucci, A.; Mulvaney, P. *Adv. Mater.* **2008**, *20*, 69−73.

(6) (a) Rademacher, A.; Maerkle, S.; Langhals, H. *Chem. Ber.* **1982**, *115*, 2927−2934. (b) Nagao, Y.; Misono, T. *Dyes Pigm.* **1984**, *5*, 171−188. (c) Zollinger, H. *Color Chemistry*; VCH: Weinheim, 1987. (d) Würthner, F. *Chem. Commun.* **2004**, 1564−1579.

(7) Hernando, J.; de Witte, P. A. J.; van Dijk, E. M. H. P.; Korterik, J.; Nolte, R. J. M.; Rowan, A. E.; Garcia-Parajó, M. F.; van Hulst, N. F. *Angew. Chem., Int. Ed.* **2004**, *43*, 4045−4049.

(8) (a) Schmidt-Mende, L.; Fechtenkötter, A.; Müllen, K.; Moons, E.; Friend, R. H.; MacKenzie, J. D. *Science* **2001**, *293*, 1119−1122. (b) Cremer, J.; Mena-Osteritz, E. M.; Pschierer, N. G.; Müllen, K.; Bauerle, P. *Org. Biomol. Chem.* **2005**, *3*, 985−995. (c) Cremer, J.; Bauerle, P. *J. Mater. Chem.* **2006**, *16*, 874−884.

(9) Li, Y.; Wang, Z. H. *Org. Lett.* **2009**, *11*, 1385−1387.

(10) (a) Peeters, E.; van Hal, P. A.; Meskers, S. C. J.; Janssen, R. A. J.; Meijer, E. W. *Chem.—Eur. J.* **2002**, *8*, 4470−4474. (b) Hippius, C.; Schlosser, F.; Vysotsky, M. O.; Bohmer, V.; Wurthner, F. *J. Am. Chem. Soc.* **2006**, *128*, 3870−3871. (c) Weil, T.; Reuther, E.; Müllen, K. *Angew. Chem., Int. Ed.* **2002**, *41*, 1900−1904.

(11) (a) Petritsch, K.; Dittmer, J. J.; Marseglia, E. A.; Friend, R. H.; Lux, A.; Rozenberg, G. G.; Moratti, S. C.; Holmes, A. B. *Sol. Energy Mater. Sol. Cells* **2000**, *61*, 63−72. (b) Dittmer, J. J.; Lazzaroni, R.; Leclère, P.; Moretti, P.; Ganström, M.; Petritsch, K.; Marseglia, E. A.; Friend, R. H.; Brédas, J. L.; Rost, H.; Holmes, A. B. *Sol. Energy Mater. Sol. Cells* **1999**, *61*, 53−61.

(12) (a) Avlasevich, Y.; Müllen, K. *Chem. Commun.* **2006**, 4440−4442. (b) Pschirer, N. G.; Kohl, C.; Nolde, F.; Qu, J.; Müllen, K. *Angew. Chem., Int. Ed.* **2006**, *45*, 1401−1404.

(13) (a) Oliveira, S. L.; Corrêa, D. S.; Misoguti, L.; Constantino, C. J. L.; Aroca, R. F.; Zilio, S. C.; Mendonca, C. R. *Adv. Mater.* **2005**, *17*, 1890−1893. (b) Corrêa, D. S.; Oliveira, S. L.; Misoguti, L.; Zilio, S. C.; Aroca, R. F.; Constantino, C. J. L.; Mendonca, C. R. *J. Phys. Chem. A* **2006**, *110*, 6433−6438. (c) Belfield, K. D.; Bondar, M. V.; Hernandez, F. E.; Przhonska, O. V. *J. Phys. Chem. C* **2008**, *112*, 5618−5622.

(14) (a) Zhao, Y.; Ren, A. M.; Feng, J. K.; Sun, C. C. *J. Chem. Phys.* **2008**, *129*, 014301−1. (b) Liu, X. T.; Zhao, Y.; Ren, A. M.; Feng, J. K. *J. Mol. Model.* **2011**, *17*, 1413−1425.

(15) (a) Quante, H.; Müllen, K. *Angew. Chem., Int. Ed.* **1995**, *34*, 1323−1325. (b) Geerts, Y.; Quante, H.; Platz, H.; Mahrt, R.; Hopmeier, M.; Böhm, A.; Müllen, K. *J. Mater. Chem.* **1998**, *8*, 2357−2369. (c) Langhals, H.; Büttner, J.; Blanke, P. *Synthesis* **2005**, 364−366. (d) Tam-Chang, S. W.; Seo, W.; Iverson, I. K. *J. Org. Chem.* **2004**, *69*, 2719−2726. (e) Pschirer, N. G.; Kohl, C.; Nolde, F.; Qu, J.; Müllen, K. *Angew. Chem., Int. Ed.* **2006**, *45*, 1401−1404.

(16) (a) Jones, B. A.; Ahrens, M. J.; Yoon, M. H.; Facchetti, A.; Marks, T. J.; Wasielewski, M. R. *Angew. Chem., Int. Ed.* **2004**, *43*, 6363−6366. (b) Würthner, F.; Osswald, P.; Schmidt, R.; Kaiser, T. E.; Mansikkamäki, H.; Könemann, M. *Org. Lett.* **2006**, *8*, 3765−3768.

(17) Qian, H.; Liu, C. M.; Wang, Z. H.; Zhu, D. B. *Chem. Commun.* **2006**, 4587−4589.

(18) (a) Jiang, W.; Qian, H.; Li, Y.; Wang, Z. *J. Org. Chem.* **2008**, *73*, 7369−7372. (b) Zhen, Y.; Qian, H.; Xiang, J.; Qu, J.; Wang, Z. *Org. Lett.* **2009**, *11*, 3084−3087. (c) Li, Y.; Wang, Z. *Org. Lett.* **2009**, *11*, 1385−1388. (d) Qian, H.; Yue, W.; Zhen, Y.; Motta, S. D.; Donato, E. D.; Negri, F.; Qu, J.; Xu, W.; Zhu, D.; Wang, Z. *J. Org. Chem.* **2009**, *74*, 6275−6282. (e) Li, Y.; Gao, J.; Motta, S. D.; Negri, F.; Wang, Z. H. *J. Am. Chem. Soc.* **2010**, *132*, 4208−4213.

(19) (a) Jiao, C. J.; Huang, K.-W.; Luo, J.; Zhang, K.; Chi, C. Y.; Wu, J. S. *Org. Lett.* **2009**, *11*, 4508−4511. (b) Jiao, C. J.; Huang, K.-W.; Guan, Z. P.; Xu, Q.-H.; Wu, J. S. *Org. Lett.* **2010**, *12*, 4046−4049.

(20) Frisch, M. J. et al. *Gaussian 09, Revision B.01*; Gaussian Inc.: Wallingford, CT, 2010.

(21) (a) Becke, A. D. *J. Chem. Phys.* **1993**, *98*, 5648. (b) Becke, A. D. *Phys. Rev. A* **1988**, *38*, 3098−3100. (c) Lee, C.; Yang, W.; Parr, R. G. *Phys. Rev. B* **1988**, *37*, 785−789.

(22) (a) Cances, E.; Mennucci, B.; Tomasi, J. *J. Chem. Phys.* **1997**, *107*, 3032−3041. (b) Cossi, M.; Barone, V.; Cammi, R.; Tomasi, J. *Chem. Phys. Lett.* **1996**, *225*, 327−335. (c) Miertus, S.; Tomasi, J. *Chem. Phys.* **1982**, *65*, 239−245. (d) Miertus, S.; Scrocco, E.; Tomasi, J. *Chem. Phys.* **1981**, *55*, 117−129.
(23) Cha, M.; Torruellas, W. E.; Stegeman, G. I.; Horsthuis, W. H. G.; Möhlmann, G. R.; Meth, J. *Appl. Phys. Lett.* **1994**, *65*, 2648−2650.
(24) Kogej, T.; Beljonne, D.; Meyers, F.; Perry, J. W.; Marder, S. R.; Brédas, J. L. *Chem. Phys. Lett.* **1998**, *298*, 1−3.
(25) Orr, B. J.; Ward, J. F. *Mol. Phys.* **1971**, *20*, 513−526.
(26) Bishop, D. M.; Luis, J. M.; Kirtman, B. *J. Chem. Phys.* **2002**, *116*, 9729−9379.
(27) Beljonne, D.; Wenseleers, W.; Zojer, E.; Shuai, Z.; Vogel, H.; Pond, S. J. K.; Perry, J. W.; Marder, S. R.; Brédas, J. L. *Adv. Funct. Mater.* **2002**, *12*, 631−641.
(28) Albota, M.; Beljonne, D.; Brédas, J. L.; Ehrlich, J. E.; Fu, J. Y.; Heikal, A. A.; Hess, S. E.; Kogej, T.; Levin, M. D.; Marder, S. R.; McCord-Maughor, D.; Perry, J. W.; Röckel, H.; Rumi, M.; Subramaniam, G.; Webb, W. W.; Wu, X. L.; Xu, C. *Science* **1998**, *281*, 1653−1656.
(29) Zhao, Y.; Ren, A.-M.; Feng, J.-K.; Zhou, X.; Ai, X.-C.; Su, W.-J. *Phys. Chem. Chem. Phys.* **2009**, *11*, 11538−11545.
(30) Liu, X.-T.; Zou, L.-Y.; Ren, A.-M.; Guo, J.-F.; Sun, Y.; Huang, S.; Feng, J.-K. *Theor. Chem. Acc.* **2011**, *130*, 37−50.
(31) Zhang, H. C.; Guo, E. Q.; Zhang, Y. L.; Ren, P. H.; Yang, W. J. *Chem. Mater.* **2009**, *21*, 5125−5135.
(32) Òscar, R. P.; Luo, Y.; Ågren, H. *J. Chem. Phys.* **2006**, *124*, 094310−1.
(33) Ma, W. B.; Wu, Y. Q.; Gu, D. H.; Gan, F. X. *J. Mol. Struct. (THEOCHEM)* **2006**, *772*, 81−87.
(34) Litani-Barzilai, I.; Bulatov, V.; Schechter, I. *Anal. Chim. Acta* **2004**, *501*, 151−156.
(35) Lukeš, V.; Aquino, A.; Lischka, H. *J. Phys. Chem. A* **2005**, *109*, 10232−10238.
(36) Peng, Q.; Niu, Y.; Wang, Z.; Jiang, Y.; Li, Y.; Liu, Y.; Shuai, Z. *J. Chem. Phys.* **2011**, *134*, 074510−1−10.
(37) Rumi, M.; Ehrlich, J. E.; Heikal, A. A.; Perry, J. W.; Barlow, S.; Hu, Z.-Y.; McCord-Maughon, D.; Parker, T. C.; Röckel, H.; Thayumanavan, S.; Marder, S. R.; Beljonne, D.; Brédas, J.-L. *J. Am. Chem. Soc.* **2000**, *122*, 9500−9510.
(38) Ray, P. C.; Leszczynski, J. *J. Phys. Chem. A* **2005**, *109*, 6689−6696.